Analytical Methods

PAPER

View Article Online
View Journal | View Issue

Cite this: *Anal. Methods*, 2019, **11**, 2650

An "on–off–on" fluorescent nanoprobe for recognition of Cu^{2+} and GSH based on nitrogen co-doped carbon quantum dots, and its logic gate operation†

Yifang Gao, Huilin Zhang, Shaomin Shuang, Hui Han* and Chuan Dong*

Novel nitrogen co-doped carbon dots (NCDs) were synthesized as a fluorescent "on–off–on" switch for the highly sensitive and selective sensing of Cu^{2+} and glutathione (GSH) by a straightforward pyrolysis route. The as-prepared NCDs exhibited not only high optical stability but also superior biocompatibility and biolabeling potentials. The "on–off" process was realized by the introduction of Cu^{2+} on luminescent NCDs, which formed an NCDs–Cu^{2+} complex and quenched the fluorescence of NCDs efficiently. "Off–on" was also recovered upon addition of GSH owing to the competitive binding of GSH and Cu^{2+} leading Cu^{2+} to escape from the surface of the NCDs. The probe demonstrated high sensitivity and selectivity toward Cu^{2+} and GSH over other analytes, with a low detection limit of 3.62×10^{-4} μM and 6.32×10^{-4} μM, respectively. Concurrently, an "AND" logic gate was constructed based on the as-fabricated NCDs. Thanks to the highly intense emission of NCDs, the gradual quenching and restoration of their fluorescence with the addition of Cu^{2+} and further GSH could also be observed with the naked eye. More importantly, the probe was also extended to cellular imaging. The probe demonstrates high selectivity, repeatability, and stability, which offers a promising platform for environmental and biological sensing applications.

Received 28th February 2019
Accepted 20th April 2019

DOI: 10.1039/c9ay00424f

rsc.li/methods

Introduction

Copper ions (Cu^{2+}) play remarkably important roles in various physiological processes, and are the third copious transition metal ion in the human body.[1] Various redox reactions are catalyzed that depend on a copper enzyme in the cytoplasm and mitochondria in the cytoplasm and mitochondria.[2] Therefore, the detection of Cu^{2+} is an important concern. As far as we know, either a deficiency or an excess of copper will cause some diseases in human health, such as hematological manifestations,[3] neurological problems,[4] gastrointestinal disturbance[5] and damage of the liver and kidneys.[6] Therefore, an efficient method for selectively probing Cu^{2+} is highly meaningful in biological and environmental systems. Current analytical techniques for Cu^{2+} include the colorimetric method,[7] surface-enhanced Raman scattering,[8] atomic absorption spectroscopy (AAS),[9] inductively-coupled plasma-mass spectrometry (ICP-MS),[10] polarography,[11] the chemiluminescent method[12] and the electrochemical method;[13] however, drawbacks of these techniques, including the need for specialized and expensive equipment, time-consuming pretreatments and tedious procedures, still remain. Very recently, numerous researchers have developed valid fluorescence probes to discriminate Cu^{2+}. For example, Wang *et al.*[14] fabricated a "turn-off" fluorescent sensor based on Au–AgNCs for specifically recognizing Cu^{2+}. From then on, other literature also reported the fluorescent probe (QG@PDA,[15] AgNCs-BSA@ZIF-8 (ref. 16) and pyrene-based fluorescent chemosensor[17]) for recognition of Cu^{2+}. The considerable efforts of these pioneers have had active impacts on fluorescent probes as a platform for discriminating Cu^{2+}. It is expected that an excellent advantageous fluorescent probe will eventually be developed.

Reduced glutathione (GSH), an important tripeptide thiol, plays a key role in biological systems containing the maintenance of intracellular redox states, metabolism and detoxification.[14] Abnormal levels of GSH are related to an assortment of diseases, such as Parkinson's,[18] HIV,[19] aging,[20] cancer[21] and autism in children.[22] Moreover, due to its important physiological properties as an antioxidant and antidote,[23] it has been commonly used in pharmaceuticals, cosmetics industries and health foods.[24] These examples demonstrate the need to develop quantitative and qualitative methods for the detection of GSH. Currently, major detection techniques for GSH are high-performance liquid chromatography (HPLC),[25] electrochemiluminescence,[26] surface-enhanced Raman scattering

Department Institute of Environmental Science, School of Chemistry and Chemical Engineering, Shanxi University, Taiyuan, 030006, China. E-mail: dc@sxu.edu.cn; Fax: +86-351-7018613; Tel: +86-351-7018613

† Electronic supplementary information (ESI) available. See DOI: 10.1039/c9ay00424f

(SERS),[27] electrochemistry (EC),[28] capillary electrophoresis (CE),[29] enzyme-linked immunosorbent assay (ELISA)[30] and so on. Although these strategies have shown promising results for GSH detection, there are still some disadvantages, including the need for expensive equipment, time-consumption and complex sample pretreatment. In order to develop alternative methods to overcome these limitations, more and more attention has been focused on fluorescent sensors based on their extremely high sensitivity, ease of operation and real-time detection.[31] Various innovative fluorescent nano-materials including gold nanoparticles,[32] fluorescent semiconductor quantum dots (QDs)[33] and upconversion nanoparticles (UCNPs)[34] have been broadly constructed for the detection of diverse substances. For example, Wang *et al.*[35] synthesized melamine–copper nanocomposites by the controlled supermolecular self-assembly for probing GSH based on the displacement reaction route. Ma *et al.*[36] employed a DNA probe for the detection of biothiols (glutathione and cysteine). In addition, Wang *et al.*[37] also manufactured Ag–ZnO nanorods for ultrasensitive and high-throughput electroanalysis of glutathione in HeLa cells. Among these available materials, some drawbacks for UCNPs, including the need for special equipment, complex sample pretreatment and cutting-edge technology still remain, which might limit their application in routine assays. In addition, not only do the QD involve heavy metals, but the required methods are often also extraordinarily complicated and tremendously time consuming. Furthermore, with respect to AuNPs, despite the outstanding characters such as superior sensitivity, handy readout and so on, drawbacks including very low quantum yield and expensive material are obvious. Therefore, an efficient nanomaterial is highly desirable.

Recently, as an emerging fluorescent carbon nanomaterial, CDs have opened up a novel perspective for detection of GSH on account of their distinct features compared with traditional fluorescent nanomaterial, such as an outstanding optical nature, excellent chemical stability, biocompatibility and low toxicity.[38,39] For example, Gu *et al.*[40] fabricated a ternary system of fluorophore surfactant assembly-Au(III) for discriminating responses to GSH with the limit of detection of 2.02 μM by charge transfer. Guo *et al.*[41] constructed sensing platform based-CDs for the sequential detection of Cu^{2+} and GSH. These studies gave us inspiration. In addition, these sensors responded to all thiol-containing amino acids, and only a few could distinguish Cys/Hcy/GSH from each other. Therefore, it is of great interest to design a technique to discriminate GSH from other thiols.

In this study, we synthesized NCDs using D-glucose and L-asparagine as precursors *via* a single-step hydrothermal method. Not only can the as-synthesized NCDs exhibited superior photostability, excellent biocompatibility and low toxicity, but the NCDs are found to display a noteworthy "on–off–on" three-state emission as well with the stepwise addition of Cu^{2+} and GSH, implying potential applications as a bifunctional sensing platform. The probe demonstrated high sensitivity and selectivity to Cu^{2+} and GSH over other analytes, and the limits of detection obtained were 3.62×10^{-4} μM and 6.32×10^{-4} μM, respectively. In addition, the NCDs further exhibited capability for the highly selective and sensitive recognition of Cu^{2+} and GSH in intracellular imaging (Scheme 1). Simultaneously, an "AND" logic gate based on the as-fabricated NCDs was built, with satisfactory results. All the above outcomes suggest that NCDs have significant prospects in biosensing, disease diagnosis and environmental monitoring.

Experimental

Materials

D-Glucose, L-asparagine and amino acids containing arginine (Arg), alanine (Ala), cysteine (Cys), methionine (Met), histidine (His), threonine (Thr), proline (Pro), leucine (Leu), lysine (Lys), phenylalanine (Phe), tryptophan (Trp), tyrosine (Tyr), glycine (Gly), aspartic acid (Asp), valine (Val), isoleucine (Ile), serine (Ser) and glutamic acid (Glu) were purchased from Aldrich (Milwaukee, WI, USA). KCl, NaCl, $CaCl_2$, $ZnCl_2$, $BaCl_2$, $MnCl_2$, $AlCl_3$, $CrCl_3$, $AgNO_3$, $Mg(NO_3)_2$, $Cu(NO_3)_2$, $Ni(NO_3)_2$, $Co(NO_3)_2$, $Cd(NO_3)_2$, $Pb(NO_3)_2$, $Hg(NO_3)_2$, $Fe(NO_3)_3$ and $FeSO_4$ were obtained from Aladdin Ltd (Shanghai, China). Dimethyl sulfoxide (DMSO), Dulbecco's modified Eagle's medium (DMEM), fetal bovine serum (FBS), trypsin, ethylenediamine tetraacetic acid (EDTA) and 3-(4,5-dimethylthiazol-2-yl)-2,5-diphenyltetrazolium bromide (MTT) were purchased from Solarbio (Beijing, China). Other reagents were taken from Beijing Chemical Reagents Company (Beijing, China). All chemicals used were analytical reagent grade and were used without further purification. In all experiments, the water was treated as ultrapure water (≥18.25 MΩ cm) from a molecular purification system (Shanghai, China).

Preparation of CDs

Glucose (0.45 g) and L-asparagine (0.33 g) were loaded into a beaker and 1 M NaOH (3.0 mL) was added. The reaction mixture was sufficiently mixed *via* sonication and kept for 30 min, then heated to 150 °C and maintained for 10 min. The final reaction products were completely dissolved into 10 mL water, and then subjected to dialysis *via* a dialysis membrane (MWCO = 500–1000) for 24 h after filtering to remove small molecules. The NCDs in the dialysis bag were freeze-dried to obtain a brown solid.

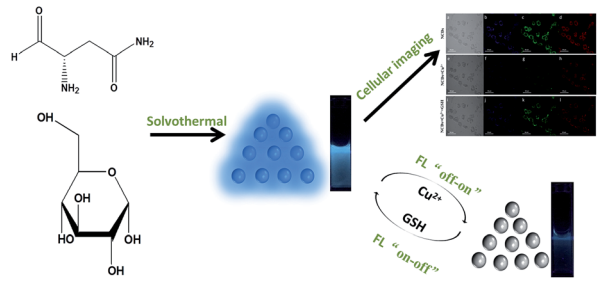

Scheme 1 Schematic illustration for the synthetic procedure of NCDs and application.

Detection of Cu^{2+} and GSH

The as-synthesized NCDs powder was dissolved in a phosphate buffer saline (PBS comprising 134 mM NaCl, 2.7 mM KCl, 8.0 mM Na_2HPO_4 and 2.0 mM KH_2PO_4) solution (pH 7.4) at a concentration of 0.25 mg mL^{-1}. In order to detect Cu^{2+}, different concentrations of Cu^{2+} were separately added into the NCDs solution, and then the fluorescence spectra of the detected Cu^{2+} were recorded (λ_{ex} at 391 nm). In order to detect GSH, the NCDs solution (0.25 mg mL^{-1}) was first mixed with Cu^{2+} (40 μM), and then diverse concentrations of GSH were added. Then, the fluorescence spectra were recorded. For further survey of the selectivity and interference of NCDs in Cu^{2+} detection, different metal ions (K^+, Na^+, Ca^{2+}, Zn^{2+}, Ba^{2+}, Mn^{2+}, Al^{3+}, Cr^{3+}, Ag+, Mg^{2+}, Cu^{2+}, Ni^{2+}, Co^{2+}, Pb^{2+}, Hg^{2+}, Fe^{3+} and Fe^{2+}) were applied in the selectivity experiments. To evaluate the selectivity of the NCDs probe, 10 μL of each of the above ion solutions (0.1 mol L^{-1}) was mixed with 1.99 mL of NCDs (0.25 mg mL^{-1}), and the PL intensities were measured under excitation at 391 nm, and the emission intensity at 475 nm was recorded for quantitative analysis. To evaluate the selectivity of the sensor for GSH, amino acids (Arg, Ala, Cys, Met, His, Thr, Pro, Leu, Lys, Phe, Trp, Tyr, Gly, Asp, Val, Ile, Ser and Glu) were added in place of GSH, and the same detection situations were chosen, as mentioned above.

Results and discussion

Characterization of the CDs

The transmission electron microscopy (TEM) image (Fig. 1A) was fully examined in terms of size and morphology of the as-prepared CDs. The CDs were sphere-shaped, with an average particle size of 2.80 nm. Fig. 1B shows a histogram of the size distribution of CDs whose size varies from 1 to 5 nm based on the count of about 200 CDs obtained correspondingly. High-resolution TEM reveals that CDs hold well-resolved lattice spacing value of 0.21 nm (inset Fig. 1A), which matches up the (100) diffraction facets of graphite.[42]

Surface analysis of NCDs was carried out using X-ray photoelectron spectroscopy (XPS) (Fig. 1C). C 1s, N 1s and O 1s peaks were observed at 282.1, 396.6 and 530.9 eV, respectively. The high-resolution XPS spectrum of C 1s (Fig. S1A†) can be well deconvolved into three components, corresponding to sp^2 C atoms in C=C/C–C at 284.8 eV, sp^3 carbons in C–N/C–O at 286.8 eV and a carboxyl group (CO_2H) at 288.2 eV, respectively. In the N 1s spectrum of the NCDs, three peaks at 398.9, 399.6 and 400.4 eV are attributed to pyridinic N, pyrrolic N and N–$(C)_3$, respectively (Fig. S1B†). Fig. S1C† depicts the O 1s spectrum associated with two peaks at 531.8 and 532.9 eV, which are related to C–OH and C=O, respectively.[43,44] The elemental analysis results provided in Table S1† reveal that the NCDs comprised of C 41.5, H 4.8, N 9.0 and O (calculated) 44.7 wt%, signifying that the as-prepared NCDs are nitrogen doped.

Fourier transform infrared (FT-IR) spectroscopy (Fig. 1D) was conducted to recognize the surface functional groups existing on the NCDs surface. The existence of a broad peak centered at 3093–3720 cm^{-1} signifies the stretching vibrations of O–H and N–H bonds, showing the presence of hydroxyl and amino groups.[45,46] The stretching vibration peak of C–H is exhibited by the absorption band at 2930 cm^{-1}. Three sharp peaks at 1678, 1596 and 1392 cm^{-1} are ascribed to the stretching vibrations of C=O, C=N and N–H vibration, respectively. The tiny peak is assigned to the stretching vibrations of C–O–C at 1304 cm^{-1}. The peaks at 1085 cm^{-1} are attributed to C–OH stretching. The presence of polar functional groups on the surfaces of NCDs makes it possible for them to be readily dispersed in water. FT-IR identify surface functional groups consistent with XPS.

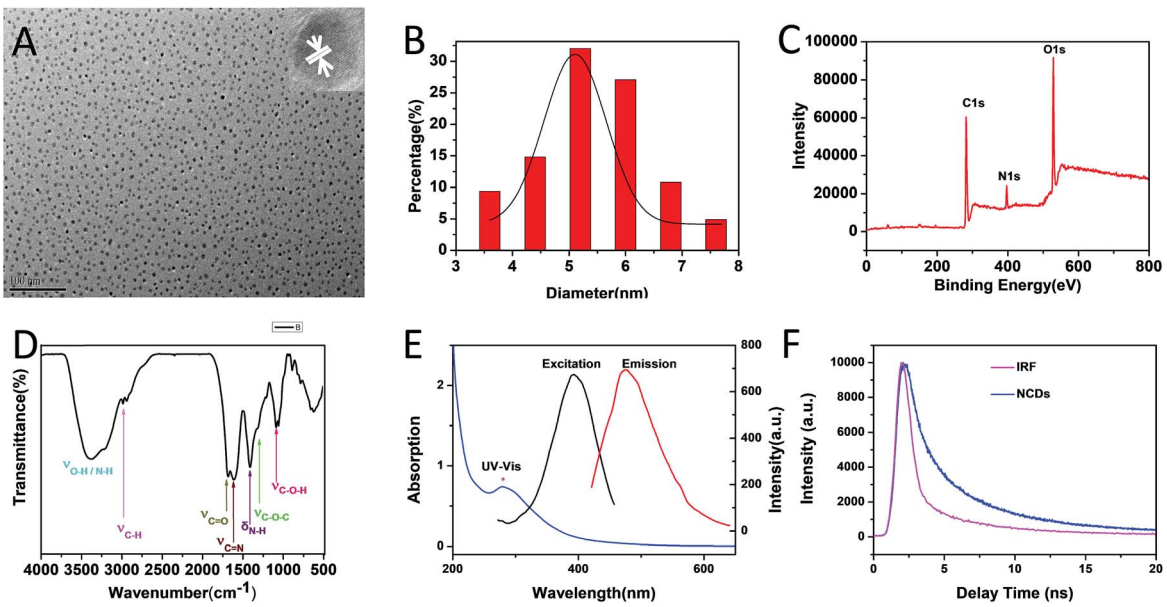

Fig. 1 (A) TEM and (inset) the size distribution of the NCDs. (B) High-resolution TEM images of the NCDs. (C) FT-IR, (D) XPS spectra, (E) UV-vis absorption and FL spectra of the NCDs. (F) Fluorescence lifetime of NCDs. The concentrations of NCDs samples are 0.25 mg mL^{-1}.

Subsequently, the photoluminescence natures of the as-synthesized NCDs are examined. A widespread absorption band at 256–400 nm was noted in the ultraviolet-visible (UV-vis) absorption spectrum (Fig. 1E), which can be matched to the π–π* transition of the C=C bond and the n–π* transition of the π system, excluding the C=O and C=N bonds. As shown in Fig. 1E, the NCDs are observed to emit blue light with optimum excitation and emission wavelengths at 391 nm and 475 nm, respectively. The excitation-dependent photoluminescence (Fig. S2†) behavior may be due to the inclusion of multiple C-, N- and O- functional groups on the surface of the NCDs that are capable of producing a variety of surface states with various energy levels and emission traps.[47] In addition, the excitation-dependent nature was observed with different concentrations of NCDs, which are analogous to those of formerly described CDs.[48–50] The quantum yield in sulfuric acid is calculated to be 22.16% by choosing quinine sulfate (QY = 54% in sulfuric acid) as the reference at $\lambda_{ex}/\lambda_{em}$ of 391/420–650 nm. In Fig. 1F, the fluorescence decay of NCDs was measured to be 4.35 ns, with bi-exponential decays under excitation of 391 nm. The high resistance to photo-bleaching of the NCDs was shown in Fig. S3.† The fluorescence intensity demonstrated nearly no noticeable alteration even after 180 min exposure to xenon arc light, indicating the wonderful photostability of the fluorescent probe. The NCDs powder sample for the fluorescent probe could be continually re-dispersed in water aggregation-free. There still exists great potential for carriage and conservation. In ambient conditions for 3 months, the obtained NCDs solution is not only a homogeneous phase, but has no obvious precipitation, demonstrating the long-term colloidal stability of the NCDs. The NCDs revealed superior endurance even under high ionic-strength surroundings (Fig. S4†) and independently across extensive pH ranges (2–12) (Fig. S5†). It deserves to be mentioned that NCDs reveal a concentration-dependent luminescence phenomenon, in which the maximum excitation wavelength is red-shifted from 378 nm to 634 nm, with the highest emission wavelength shifting from 468 nm to 705 nm with an increase in concentration from 0.1 mg mL^{-1} to 100 mg mL^{-1} (Fig. S6†).[51] The longer excitation/emission wavelength could bestow CDs with the ability to be detected when they penetrate into deeper tissues,[52] thus demonstrating potential for practical applications.

Fluorescence quenching of NCDs by Cu^{2+}

Through extensive screening, the fluorescence of as-prepared NCDs was discovered to display dramatic quenching in the presence of Cu^{2+}. We investigated the selectivity of NCDs as a probe for the detection of Cu^{2+} the response of the sensing system on various metallic ions under the same conditions (Fig. 2A). As revealed in Fig. 2B, the fluorescence of NCDs can be vividly quenched by Cu^{2+} and the bottom right inset of Fig. 2B is a photograph of the NCDs solution taken under a UV lamp (365 nm). In Fig. 2C, the emission spectra of NCDs decreased gradually at 475 nm with the increase in the concentration of Cu^{2+}. Furthermore, outstanding linear relationships between the quenching efficiency and concentration Cu^{2+} in the range from 0.004 to 0.1 μM and 0.6 to 222 μM are observed (Fig. 2C inset and S7†), with a linear regression of 0.990 and 0.991, respectively. The detection limit of NCDs for Cu^{2+} ions at a signal-to-noise ratio of 3 was 3.62×10^{-4} μM,[53] which is lower than most reported data (Table S2†). The linear range meets the requirement for *in vivo* imaging and sensing of Cu^{2+} ions, because the concentration of intracellular Cu^{2+} ions is reported to be around 10 μM.[54] These outcomes prove that the NCDs could be possibly used as a selective and sensitive probe for Cu^{2+} in intracellular systems.

Fluorescence restoring of the NCDs by GSH

The effect of diverse concentrations of GSH on the fluorescence of the NCDs–Cu^{2+} system was studied under suitable conditions. Fig. 2E shows the emission spectra of the NCDs–Cu^{2+} with different concentrations of GSH, and the fluorescence of the NCDs–Cu^{2+} system regularly increased. Fig. 2F and S8† show the linear relationship within the GSH concentration range from 0.003 to 0.33 μM and 1 μM to 154 μM, with a detection limit of 6.32×10^{-4} μM. In addition, we found that the emission spectra show a double peak. According to the literature, we infer that the reason may be due to the formation of multiple fluorescent complexes when GSH and NCDs–Cu^{2+} are complexed, resulting in the double peak.[55] Such a detection limit was comparable to the most sensitive method reported recently for detection of thiols. The comparison of different methods for the determination of GSH also has already been shown in Table S6.† Further, the limit of detection is much lower than the thiol content in human serum,[41] which suggests the present approach has great potential for diagnostic purposes. To investigate the selectivity of NCDs as a probe for the detection of GSH, we surveyed the spectral responses of the probe toward other amino acids (Fig. 2D). The results show that CDs–Cu^{2+} are highly selective toward GSH over the other amino acids. Moreover, the influence of H_2S and other anions on the relative fluorescence intensity of NCDs–Cu^{2+} were explored in Fig. S15,† which demonstrated neglectable variation on the NCDs–Cu^{2+} system.

Mechanism

Based on the findings mentioned above, one extraordinarily important finding is that the as-prepared NCDs were found to exhibit a diverting "on–off–on" three-state emission with the stepwise addition of Cu^{2+} and GSH by the fluorescent detection method. The outline of the mechanism of the developed sensor for Cu^{2+} is exhibited in Fig. 2. The fluorescence of the NCDs was dramatically quenched by Cu^{2+} because the transition metal copper owns half-filled energy levels (d orbitals) available for the switch of electrons with the photoexcited NCDs, the fluorescence quenching possibly due to the electron transfer between Cu^{2+} and the NCDs to accelerate the nonradiative recombination.[56] It is a well-known fact that Cu^{2+} ions tend to interact with carboxylate and amino groups *via* electron transfer.[57,58] With further addition of GSH to the NCDs–Cu^{2+} system, Cu^{2+} ions escape from the surface of NCDs due to the binding preference of Cu^{2+}, by forming a Cu–S bond (Scheme 2). A control experiment recommended no effect on GSH in the fluorescence of the NCDs in the absence of Cu^{2+}, thus the recovered fluorescence

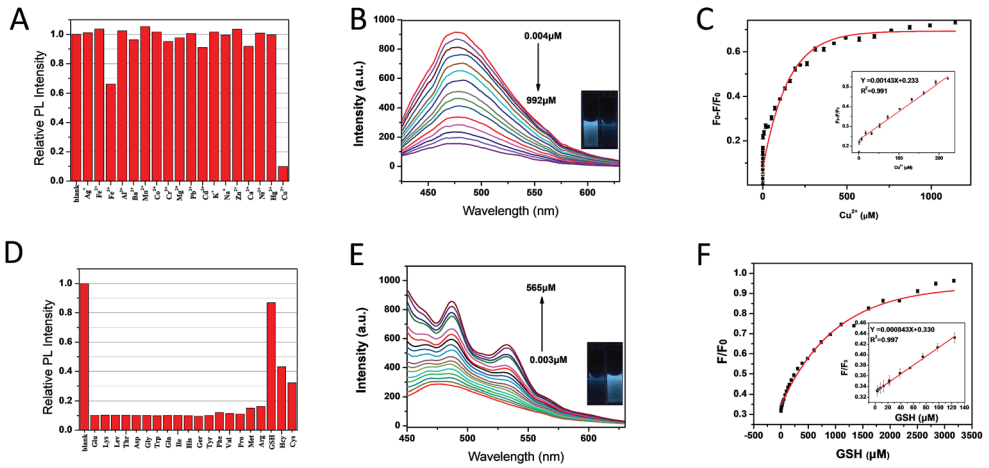

Fig. 2 (A) Influence of different metal ions on the fluorescence of NCDs. (B) Fluorescence of NCDs upon addition of various concentrations of Cu^{2+}. (C) Fluorescence quenching of NCDs in the presence of Cu^{2+} (0.004–1142 μM) and inset (C) plot of NCDs to various concentrations of Cu^{2+} where $F_0 - F/F_0$ are the PL intensities of NCDs in the absence and presence of Cu^{2+}, respectively. (D) Influence of different amino acids on the fluorescence of NCDs–Cu^{2+}. (E) Fluorescence of NCDs–Cu^{2+} upon addition of various concentrations of GSH. (E) Fluorescence recovering of NCDs in the presence of GSH (0.003–565 μM) and inset (F) plot of NCDs to various concentrations of GSH where F_0/F are the PL intensities of NCDs–Cu^{2+} in the absence and presence of GSH, respectively. The concentrations of NCDs, Cu^{2+} and GSH samples are 0.25 mg mL^{-1}, 10.0 mM and 10.0 mM, respectively.

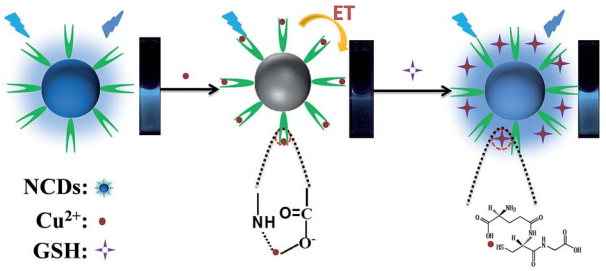

Scheme 2 Schematic illustration of the detection strategy for Cu2+ and GSH activity based on NCDs.

might be due to the interface between GSH and Cu^{2+}, which then affected the emission of the NCDs (Fig. S9†).

For further exploration of the character of the three-state emission course, UV-vis spectroscopy, FT-IR spectroscopy and fluorescence lifetime measurements were engaged to offer further insights into the possible mechanism. The FT-IR spectrum of the NCDs–Cu^{2+} system shows that the stretching vibration and bending vibration of N–H blue shifted by 61 cm^{-1} and 14 cm^{-1} with respect to that of the initial NCDs, respectively (Fig. S10†). In addition, the IR spectrum of glutathione was also compared, and this result was verified again. However, the C–H stretching vibration at 2930 cm^{-1} does not show any shift, suggesting that the fluorescence quenching may be partly attributed to the amino coordination with Cu^{2+}. In the FT-IR spectrum of the NCDs–Cu^{2+} system, an absorption band at 3207 cm^{-1} disappears due to the carboxylate of the NCDs surface bound to Cu^{2+}. The UV-vis spectrum of the NCDs–Cu^{2+}, shown in Fig. S11,† exhibited a new absorption band at 665 nm. This band was triggered by the N → Cu ligand-to-metal charge transfer. In addition, the photoluminescence extinguishing mechanism of the scheme was explored by the calculated fluorescence decay dynamics. The fluorescence decay curves of CDs, NCDs–Cu^{2+} can be fitted by a double-exponential formula, comprising the lifetime τ_1 and τ_2. As shown in Fig. S12 and Table S3,† the average lifetime of NCDs is calculated as 4.35 ns. After coordination with Cu^{2+} ions, the lifetime is reduced to 1.97 ns. The decrease in the lifetime indicates an ultrafast NCDs–Cu^{2+} electron-transfer process and leads to dynamic quenching.[59] These results indicate the quenching progress owing to the exceptional coordination interaction between Cu^{2+} and the carboxylate and amino groups of the NCDs surface, which has been used for the recognition of metal ions or colored reactions in traditional organic chemistry.[60] As shown in Fig. S12 and Table S3,† the average lifetime of NCDs–Cu^{2+} is calculated to be 1.97 ns. After coordination with GSH, the lifetime is increased to 3.47 ns. The results further indicate that the recovery of the lifetime was due to Cu^{2+} ions that escaped from the surface of NCDs. The zeta potential also provided a better understanding of the mechanism. As shown in Table S4,† the NCDs were −8.59 mV; after the addition of Cu^{2+}, the zeta potential value was shifted to −3.31 mV. Thus, we presumed that Cu^{2+} majorly interacted with carboxyl or hydroxyl groups and partially shielded the negative charge.[61] Simultaneously, small amino groups might also coordinate with Cu^{2+}. With the further addition of GSH to the NCDs–Cu^{2+} system, the zeta potential value becomes −8.32 mV, further indicating that Cu^{2+} escaped from the surface of the NCDs.

In vitro cellular imaging examination

To verify the biological relevance of the NCDs-based probe, experiments were carried out to evaluate the use of the probe in the fluorescence imaging of cellular Cu^{2+} and GSH. The fluorescent nanoparticles should have both excellent optical

properties and low cytotoxicity. To estimate the cytotoxicity of the NCDs, the viability of human hepatoma carcinoma SMMC7721 cells were investigated as illustrative cell lines handled with various concentrations of NCD (the SMMC-7721 cells were donated by Prof. Xiongzhi Wu [Tianjin Medical University Cancer Institute and Hospital]). In the MTT assay, the viability remains exceeded 89% when the cells were cultured with NCDs with a concentration ranging from 0 μg mL^{-1} to 1000 μg mL^{-1} over 24 h (Fig. S13†). In addition, the cytotoxicity of NCDs–Cu^{2+} on SMMC7721 cells viability was tested. As shown in Fig. S16,† incubating NCDs with different concentrations of Cu^{2+} ranging from 0 to 100 μM, the cell viability remained greater than 80%. The above results exhibited the low toxicity of the NCDs and can be adapted for cell imaging and biological labeling. To investigate the potential application of NCDs in *in vitro* imaging of living cells, the performance as fluorescent cell labels was investigated using human hepatoma carcinoma SMMC7721 cells incubated with NCDs for 1 h. After incubating with NCDs, the human hepatoma carcinoma SMMC7721 cells were then observed with blue, green and red colors at excitation wavelengths of 405, 488 and 559 nm by laser scanning confocal microscopy (LSCM), respectively. The NCDs were well-dispersed in the cytoplasm region between the nucleus and the cell membranes, strongest blue emissions were shown in the cells stained with NCDs. As shown in Fig. 3, the emissions were barely discovered when Cu^{2+} was added into the SMMC7721 cells culture medium. The bright-field images of SMMC7721 cells incubated with NCDs, NCDs–Cu^{2+} and NCDs–Cu^{2+}–GSH (first panels in Fig. 3a, e and i) signify clearly the normal morphology of the cells, verifying that NCDs and NCDs/Cu^{2+} are biocompatible and possess minimum toxicity to the cells. The fluorescence signal could be renewed (Fig. 4A) with the addition of GSH. This observation illustrates the potential of NCDs as a bioimaging agent for living cells. These outcomes show that NCDs are efficient fluorescent probes for "on–off–on" monitoring the Cu^{2+} and GSH in live cells.

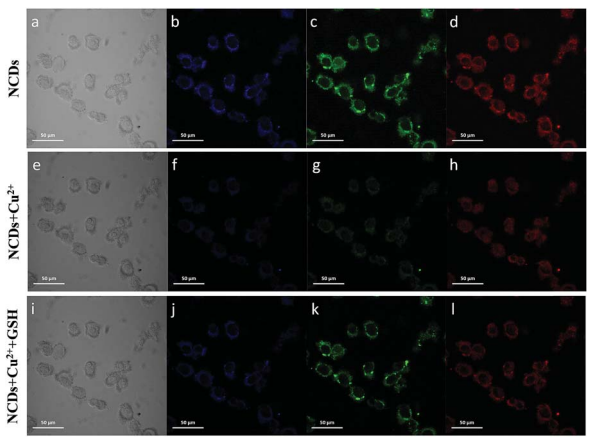

Fig. 3 Laser scanning confocal microscopy images of SMMC7721 cells, $\lambda_{ex}/\lambda_{em}$ of 405/450 ± 25, 488/535 ± 25 and 559/645 ± 25 nm, respectively. (a–d) Cells incubated with 0.25 mg mL^{-1} NCDs, (e–h) cells incubated with 0.25 mg mL^{-1} NCDs and 100 μM Cu^{2+}, (i–l) cells incubated with 0.25 mg mL^{-1}, 100 μM Cu^{2+} and 100 μM GSH. All scale bars represent 50 μm.

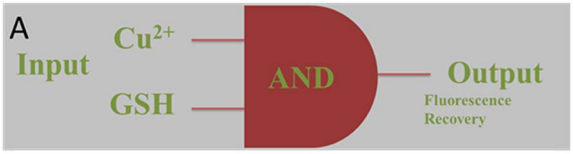

B AND logic gate

Input		Output
Cu^{2+}	GSH	FR475Intensity
0	0	0
1	0	0
0	1	0
1	1	1

Fig. 4 (A) Logic scheme of the "AND" logic gate (A) and truth table (B).

Detection of Cu^{2+} ions in real samples

To explore the applicability of this proposed method, the probe was applied to the detection Cu^{2+} in real river water samples. Using the proposed methods described above, local river water samples were analyzed by the standard addition method. The content of Cu^{2+} resulted from the standard curve and the regression equation in the river samples. All data are listed in Table S5.† The recovery of the spiked samples ranged between 99.5% and 100.2% (measurements replicated six times). This result based on the fluorometry of NCDs was compared with the results obtained using a traditional flame atomic absorption spectrometric method. As demonstrated in Table S5,† good consistency was obtained between these two methods, showing the excellent behavior of our proposed approach in real samples.

Logic operation of CDs toward Cu^{2+} and GSH

According to the three-state emission with stepwise addition of Cu^{2+} and GSH, we devised an "AND" molecular logic gate.[62,63] The two inputs were Cu^{2+} and GSH, and the optical output was the fluorescence signal recovery in this logic gate. Fig. 4 shows the homologous symbol and truth table of the results of each input mode. For the output, the definitions of "1" and "0" are the recovery of fluorescence intensity and no fluorescence recovery, respectively. For the input, the definitions of "1" is the presence of inputs (Cu^{2+} and GSH), and the definitions of "0" is the absence of inputs (Cu^{2+} and GSH). Thus, the fluorescence signal is significantly enhanced only when the system receives two inputs (1, 1), and the gate is activated and emits a "1" output signal.[64]

Conclusions

In conclusion, the NCDs were synthesized by a straightforward pyrolysis route with D-glucose and L-asparagine as precursors. A simple fluorescence sensor was constructed for the highly selective and sensitive sequential recognition of Cu^{2+} and GSH based on NCDs. The "on–off" process was realized by the introduction of Cu^{2+} on luminescent NCDs, which formed the complex of NCDs–Cu^{2+} and quenched the fluorescence of NCDs

efficiently, and recovered ("off–on") upon addition of GSH owing to the competitive binding of GSH and Cu^{2+} that allows Cu^{2+} to escape from the surface of the NCDs. The probe demonstrated high sensitivity and selectivity toward Cu^{2+} and GSH over other analytes, with a low detection limit of 3.62×10^{-4} μM and 6.32×10^{-4} μM, respectively. To the best of our knowledge, the detection limit is lower than previous reports so far. Concurrently, an "AND" logic gate has been constructed based on the as-fabricated NCDs. The gradual quenching and restoration of their fluorescence with the addition of Cu^{2+} and further GSH could also be observed with the naked eye due to the highly intense emission of NCDs. In addition, the probe was also extended to cellular imaging. The probe demonstrates high selectivity, repeatability and stability, which offers a promising platform for environmental and biological sensing applications.

Conflicts of interest

There are no conflicts to declare.

Acknowledgements

The authors gratefully acknowledge financial support from the National Natural Science Foundation of China (No. 21874087, 21705101, 21475080 and 21575084), Shanxi Province Hundred Talents Project and Shanxi Province Graduate Education Innovation Project (2017BY006).

References

1 S. P. Wu, R. Y. Huang and K. J. Du, *Dalton Trans.*, 2009, 4735–4740, DOI: 10.1039/b822613j.
2 W. Wang, Q. Yang, L. Sun, H. Wang, C. Zhang, X. Fei, M. Sun and Y. Li, *J. Hazard. Mater.*, 2011, **194**, 185–192.
3 B. B. Tewari, *J. Chem. Eng. Data*, 2010, **55**, 1779–1783.
4 S. Anbu, R. Ravishankaran, M. F. Guedes da Silva, A. A. Karande and A. J. Pombeiro, *Inorg. Chem.*, 2014, **53**, 6655–6664.
5 H. Zhu, J. Fan, J. Lu, M. Hu, J. Cao, J. Wang, H. Li, X. Liu and X. Peng, *Talanta*, 2012, **93**, 55–61.
6 R. K. Jackson, Y. Shi, X. Yao and S. C. Burdette, *Dalton Trans.*, 2010, **39**, 4155–4161.
7 A. Shahat, E. A. Ali and M. F. El Shahat, *Sens. Actuators, B*, 2015, **221**, 1027–1034.
8 D. Tsoutsi, L. Guerrini, J. M. Hermida-Ramon, V. Giannini, L. M. Liz-Marzan, A. Wei and R. A. Alvarez-Puebla, *Nanoscale*, 2013, **5**, 5841–5846.
9 S. de Oliveira Souza, L. L. François, A. R. Borges, M. G. R. Vale and R. G. O. Araujo, *Spectrochim. Acta, Part B*, 2015, **114**, 58–64.
10 A. Martín-Cameán, A. Jos, A. Calleja, F. Gil, A. Iglesias-Linares, E. Solano and A. M. Cameán, *Microchem. J.*, 2014, **114**, 73–79.
11 M. Komatsu, T. Matsueda and H. Kakiyama, *Bunseki Kagaku*, 1971, **20**, 987–992.
12 K. M. Kim, Y. H. Kim, S. H. Oh and S. H. Lee, *Luminescence*, 2013, **28**, 372–377.
13 L. Meng, Z. Fang, J. Lin, M. Li and Z. Zhu, *Talanta*, 2014, **121**, 205–209.
14 N. Zhang, Y. Si, Z. Sun, L. Chen, R. Li, Y. Qiao and H. Wang, *Anal. Chem.*, 2014, **86**, 11714–11721.
15 M. Dong, C. Liu, S. Li, R. Li, Y. Qiao, L. Zhang, W. Wei, W. Qi and H. Wang, *Sens. Actuators, B*, 2016, **232**, 234–242.
16 C. Fan, X. Lv, F. Liu, L. Feng, M. Liu, Y. Cai, H. Liu, J. Wang, Y. Yang and H. Wang, *ACS Sens.*, 2018, **3**, 441–450.
17 A. Ghorai, J. Mondal, A. K. Manna, S. Chowdhury and G. K. Patra, *Anal. Methods*, 2018, **10**, 1063–1073.
18 S. J. Chinta and J. K. Andersen, *Free Radic. Biol. Med.*, 2006, **41**, 1442–1448.
19 L. A. Herzenberg, S. C. De Rosa, J. G. Dubs, M. Roederer, M. T. Anderson, S. W. Ela, S. C. Deresinski and L. A. Herzenberg, *Proc. Natl. Acad. Sci. U. S. A.*, 1997, **94**, 1967.
20 P. S. Samiec, C. Drews-Botsch, E. W. Flagg, J. C. Kurtz, P. Sternberg, R. L. Reed and D. P. Jones, *Free Radic. Biol. Med.*, 1998, **24**, 699–704.
21 J. M. Estrela, A. Ortega and E. Obrador, *Crit. Rev. Clin. Lab. Sci.*, 2006, **43**, 143–181.
22 A. Chauhan and V. Chauhan, *Pathophysiology*, 2006, **13**, 171–181.
23 H. Sies, *Free Radic. Biol. Med.*, 1999, **27**, 916–921.
24 K. Kiriyama, K. Y. Hara and A. Kondo, *Appl. Microbiol. Biotechnol.*, 2012, **96**, 1021–1027.
25 L. Janeš, K. Lisjak and A. Vanzo, *Anal. Chim. Acta*, 2010, **674**, 239–242.
26 W.-J. Niu, R.-H. Zhu, S. Cosnier, X.-J. Zhang and D. Shan, *Anal. Chem.*, 2015, **87**, 11150–11156.
27 G. G. Huang, X. X. Han, M. K. Hossain and Y. Ozaki, *Anal. Chem.*, 2009, **81**, 5881–5888.
28 M. Shabani-Nooshabadi and F. Tahernejad-Javazmi, *RSC Adv.*, 2015, **5**, 56255–56261.
29 N. Yan, Z. Zhu, N. Ding, L. Zhou, Y. Dong and X. Chen, *J. Chromatogr. A*, 2009, **1216**, 8665–8670.
30 N. K. Wawegama, G. F. Browning, A. Kanci, M. S. Marenda and P. F. Markham, *Clin. Vaccine Immunol.*, 2014, **21**, 196–202.
31 H. Xu and M. Hepel, *Anal. Chem.*, 2011, **83**, 813.
32 Y. Shi, Y. Pan, H. Zhang, Z. Zhang, M. J. Li, C. Yi and M. Yang, *Biosens. Bioelectron.*, 2014, **56**, 39–45.
33 J. Liu, H. Chen, Z. Lin and J. M. Lin, *Anal. Chem.*, 2010, **82**, 7380–7386.
34 X. L. Zhang, C. Zheng, S. S. Guo, J. Li, H. H. Yang and G. Chen, *Anal. Chem.*, 2014, **86**, 3426.
35 Y. Hua, M. Liu, S. Li, F. Liu, Y. Cai, H. Liu, Y. Wan, X. Lv and H. Wang, *Biosens. Bioelectron.*, 2019, **124–125**, 89–95.
36 H. Zhao, M. Chen and C. Ma, *Sensors*, 2019, **19**, 934.
37 M. Liu, L. Feng, X. Zhang, Y. Hua, Y. Wan, C. Fan, X. Lv and H. Wang, *ACS Appl. Mater. Interfaces*, 2018, **10**, 32038–32046.
38 G. P. Mcdermott, J. M. Terry, X. A. Conlan, N. W. Barnett and P. S. Francis, *Anal. Chem.*, 2011, **83**, 6034–6039.
39 X. Chen, Y. Zhou, X. Peng and J. Yoon, *ChemInform*, 2010, **41**, 2120–2135.

40 J. Gu, D. Hu, W. Wang, Q. Zhang, Z. Meng, X. Jia and K. Xi, *Biosens. Bioelectron.*, 2015, **68**, 27–33.
41 Y. Guo, L. Yang, W. Li, X. Wang, Y. Shang and B. Li, *Microchim. Acta*, 2016, **183**, 1409–1416.
42 X. T. Zheng, A. Ananthanarayanan, K. Q. Luo and P. Chen, *Small*, 2015, **11**, 1620.
43 X. Jin, X. Sun, G. Chen, L. Ding, Y. Li, Z. Liu, Z. Wang, W. Pan, C. Hu and J. Wang, *Carbon*, 2015, **81**, 388–395.
44 Y.-C. Lu, J. Chen, A.-J. Wang, N. Bao, J.-J. Feng, W. Wang and L. Shao, *J. Mater. Chem. C*, 2015, **3**, 73–78.
45 X. T. Zheng, A. Ananthanarayanan, K. Q. Luo and P. Chen, *Small*, 2015, **11**, 1620–1636.
46 Q. Li, M. Zhou, Q. Yang, Q. Wu, J. Shi, A. Gong and M. Yang, *Chem. Mater.*, 2016, **28**, 8221–8227.
47 Z. Fu and F. Cui, *RSC Adv.*, 2016, **6**, 63681–63688.
48 L. Pan, S. Sun, L. Zhang, K. Jiang and H. Lin, *Nanoscale*, 2016, **8**, 17350–17356.
49 J. Shen, Y. Zhu, X. Yang and C. Li, *Chem. Commun.*, 2012, **48**, 3686–3699.
50 L. Li, G. Wu, G. Yang, J. Peng, J. Zhao and J. J. Zhu, *Nanoscale*, 2013, **5**, 4015–4039.
51 M. Zheng, S. Ruan, S. Liu, T. Sun, D. Qu, H. Zhao, Z. Xie, H. Gao, X. Jing and Z. Sun, *ACS Nano*, 2015, **9**, 11455–11461.
52 H. Li, Z. Kang, Y. Liu and S.-T. Lee, *J. Mater. Chem.*, 2012, **22**, 24230.
53 J. J. Liu, X. L. Zhang, Z. X. Cong, Z. T. Chen, H. H. Yang and G. N. Chen, *Nanoscale*, 2013, **5**, 1810–1815.
54 C. Ra, K. Furuichi, J. Rivera, J. M. Mullins, C. Isersky and N. White Kenneth, *Eur. J. Immunol.*, 1989, **19**, 1771–1777.
55 K. L. Reddy, A. M. Kumar, A. Dhir and V. Krishnan, *J. Fluoresc.*, 2016, **26**, 2041–2046.
56 C. Yuan, B. Liu, F. Liu, M. Y. Han and Z. Zhang, *Anal. Chem.*, 2014, **86**, 1123–1130.
57 J. Zong, X. Yang, A. Trinchi, S. Hardin, I. Cole, Y. Zhu, C. Li, T. Muster and G. Wei, *Biosens. Bioelectron.*, 2014, **51**, 330–335.
58 R. Sitko, B. Zawisza, E. Talik, P. Janik, G. Osoba, B. Feist and E. Malicka, *Anal. Chim. Acta*, 2014, **834**, 22–29.
59 S. Li, Y. Li, J. Cao, J. Zhu, L. Fan and X. Li, *Anal. Chem.*, 2014, **86**, 10201–10207.
60 Y. Yuan, X. Zhao, S. Liu, Y. Li, Y. Shi, J. Yan and X. Hu, *Sens. Actuators, B*, 2016, **236**, 565–573.
61 Y. Liu, W. Duan, W. Song, J. Liu, C. Ren, J. Wu, D. Liu and H. Chen, *ACS Appl. Mater. Interfaces*, 2017, **9**, 12663–12672.
62 J. Sun, F. Yang, D. Zhao, C. Chen and X. Yang, *ACS Appl. Mater. Interfaces*, 2015, **7**, 6860–6866.
63 W. Lu, Y. Gao, Y. Jiao, S. Shuang, C. Li and C. Dong, *Nanoscale*, 2017, **9**, 11545–11552.
64 L. Lu, C. Chen, D. Zhao, J. Sun and X. Yang, *Anal. Chem.*, 2016, **88**, 1238–1245.